

GRAPH-BASED FUSION FOR CHANGE DETECTION IN MULTI-SPECTRAL IMAGES

David Alejandro Jimenez-Sierra[†], Hernán Darío Benítez-Restrepo[†], Hernán Darío Vargas-Cardona[†]
Jocelyn Chanussot^{*}

[†] Pontificia Universidad Javeriana Cali

Departamento de Electrónica y Ciencias de la Computación
{davidjimenez, hbenitez, hernan.vargas}@javerianacali.edu.co

^{*} Grenoble Images Parole Signals Automatique Laboratory (GIPSA-Lab)
Grenoble Institute of Technology
jocelyn.chanussot@gipsa-lab.grenoble-inp.fr

ABSTRACT

In this paper we address the problem of change detection in multi-spectral images by proposing a data-driven framework of graph-based data fusion. The main steps of the proposed approach are: (i) The generation of a multi-temporal pixel based graph, by the fusion of intra-graphs of each temporal data; (ii) the use of Nyström extension to obtain the eigenvalues and eigenvectors of the fused graph, and the selection of the final change map. We validated our approach in two real cases of remote sensing according to both qualitative and quantitative analyses. The results confirm the potential of the proposed graph-based change detection algorithm outperforming state-of-the-art methods.

Index Terms— Change detection, data fusion, graph, multi-spectral, multi-temporal, remote sensing.

1. INTRODUCTION

Change detection (CD) refers to the task of analyzing two or more images acquired over the same area at different times (i.e., multitemporal images) in order to detect zones in which the land-cover type changed between the acquisitions [1]. CD permits to quantify the magnitude of natural disasters (i.e. floodings) and changes generated by human activity. This analysis provides fundamental data for environmental protection, sustainable development, and maintenance of ecological balance [2]. One of the most known sources of data for change detection are the Multi-spectral (MS) images that contain information from both spatial and spectral domain (i.e. Landsat series of satellites). Giving two or more co-registered images, pixel based approaches carry out change detection by probabilistic thresholding and machine learning methods [3, 4]. Even though threshold methods are efficient and useful, they are sensitive to MS image noise and require a high accuracy in the estimation of the difference image probabilistic distribution. These issues make threshold methods prone to artifacts in the final change map [5–9]. Machine

learning approaches are divided into two categories: classification and clustering. Classification methods require a multitemporal reference, which is difficult to extract from the raw data, therefore, these methods are not a practical solution [10]. Clustering techniques [11–15] are affected by parameter initialization, which may generate local minima in the learning stage. In addition, the intrinsic brightness distortion in MS images yields inaccurate change maps [4].

In order to reduce the effect of intra-class small variability and artifacts presented in MS images, we proposed a graph-based data fusion approach applied to CD. Our method extracts features from the dataset by finding eigenvectors of the normalized graph Laplacian and applying a mutual information based criteria to extract the relevant eigenvector that captures the change map. We validate our approach in two real cases: (i) a flooding, and (ii) a fire incident. Results show that our model reduces the effects of artifacts in the final change map, and it achieves low rates of false alarms in comparison to probabilistic threshold methods [5–7].

2. GRAPH BASED DATA FUSION

2.1. Graph

A graph is a non linear structural representation of data, defined by $G = (V, E)$, where G is the graph, V is a set of nodes, and E refers to the arcs or edges that explain the directed or undirected relationship between nodes. The edges have associated a weight $w_{i,j}$, that quantifies how strong the relationship is between nodes. The common measure used for each weight is a Gaussian kernel with standard deviation σ [16].

2.2. Graph-based fusion for change detection (GBF-CD)

2.2.1. Nyström extension

Given the high number of pixels in an MS image, the computational cost of calculating the full matrix $\mathbf{W} \in \mathbb{R}^{N \times N}$ is

extremely high (i.e an image with size 1280×960 is equivalent to $N = 1228800$). Therefore, an approximation of this matrix is computed through the Nyström extension [17]:

$$\mathbf{W} = \kappa_G \left(\begin{bmatrix} \mathbf{d}_{AA} & \mathbf{d}_{AB} \\ \mathbf{d}_{AB}^\top & \mathbf{C} \end{bmatrix} \right),$$

where κ_G is a Gaussian kernel, $\mathbf{d}_{AA} \in \mathbb{R}^{n_s \times n_s}$, $\mathbf{d}_{AB} \in \mathbb{R}^{n_s \times (N-n_s)}$ and $\mathbf{C} \in \mathbb{R}^{(N-n_s) \times (N-n_s)}$. This method approximates \mathbf{C} by choosing n_s samples from the dataset of size N ($n_s \ll N$), then $\mathbf{W} \approx \widehat{\mathbf{W}} = \kappa_G([\mathbf{d}_{AA}; \mathbf{d}_{AB}])^\top$. Thus, the eigenvectors of the matrix $\widehat{\mathbf{W}}$, can be spanned by eigenvalues and eigenvectors of $\kappa_G(\mathbf{d}_{AA})$. Solving the diagonalization of $\kappa_G(\mathbf{d}_{AA})$ (eigenvalues λ and eigenvectors \mathbf{U} : $\kappa_G(\mathbf{d}_{AA}) = \mathbf{U}^\top \mathbf{\Lambda} \mathbf{U}$), the eigenvectors of $\widehat{\mathbf{W}}$ can be spanned by $\widehat{\mathbf{U}} = [\mathbf{U}; \kappa_G(\mathbf{d}_{AB})^\top \mathbf{U} \mathbf{\Lambda}^{-1}]^\top$. Since the approximated eigenvectors $\widehat{\mathbf{U}}$ are not orthogonal, as explained in [17], to obtain orthogonal eigenvectors we use $\mathbf{S} = \kappa_G(\mathbf{d}_{AA}) + \kappa_G(\mathbf{d}_{AA})^{-\frac{1}{2}} \kappa_G(\mathbf{d}_{AB}) \kappa_G(\mathbf{d}_{AB})^\top \kappa_G(\mathbf{d}_{AA})^{-\frac{1}{2}}$. Then, by diagonalization of \mathbf{S} ($\mathbf{S} = \mathbf{U}_s \mathbf{\Lambda}_s \mathbf{U}_s$) the final approximated eigenvectors of \mathbf{W} are given by:

$$\widehat{\mathbf{U}} = \begin{bmatrix} \kappa_G(\mathbf{d}_{AA}) \\ \kappa_G(\mathbf{d}_{AB})^\top \kappa_G(\mathbf{d}_{AA})^{-\frac{1}{2}} \end{bmatrix} \mathbf{U}_s \mathbf{\Lambda}_s^{-\frac{1}{2}}.$$

2.2.2. Fusion step

Based on the methodology introduced in [18], where a node is understood as a pixel (i.e. image from different bands or times, also a mix of both) and it is assumed that all of the modalities are co-registered, the fusion of multi-temporal data is carried out by the procedure described in Figure 1, in which for each instance of time (X^k) the Algorithm 1 is performed.

In short, the algorithm output for one instance of time X^k corresponds to the approximate normalized adjacency matrix

Algorithm 1: GBF for temporal data

Input: Temporal images $\mathbf{X}^k \in \mathbb{R}^{m \times n}$, number of samples n_s

Output: Fused graph $\mathbf{W}_F \in \mathbb{R}^{(n_s+c) \times n_s}$

Initialize: $k = 1, N = m * n$

while $k \leq 2$ **do**

1) Take n_s samples from \mathbf{X}^k

$$X_{AA}^k = \text{sampler}(\mathbf{X}^k, n_s), \in \mathbb{R}^{n_s}$$

2) Find the complement $\bar{X}^k \in \mathbb{R}^c$ of X_{AA}^k in \mathbf{X}^k .

3) For each set X_{AA}^k and \bar{X}^k perform the pairwise distance between samples-samples

($\mathbf{d}_{AA}^k \in \mathbb{R}^{n_s \times n_s}$) and samples-complement

($\mathbf{d}_{AB}^k \in \mathbb{R}^{c \times n_s}$).

$$\mathbf{d}_{AA}^k = \left\{ \left\| x_{AA_i}^k - x_{AA_j}^k \right\|_2 \right\}_{i,j}^{n_s \times n_s}, \forall i \neq j$$

$$\mathbf{d}_{AB}^k = \left\{ \left\| \bar{x}_i^k - x_{AA_j}^k \right\|_2 \right\}_{i,j}^{c \times n_s}, \forall i \neq j$$

4) Apply the normalized graph laplacian

($\widehat{\mathbf{D}}^{-\frac{1}{2}} \widehat{\mathbf{W}} \widehat{\mathbf{D}}^{-\frac{1}{2}}$) on the distances by using the code in [17]

5) Apply a Gaussian kernel ($\kappa_G(\cdot)$) on the normalized distances and build the approximated normalized laplacian matrix based on the Nyström approximation.

$$\widehat{\mathbf{W}}_N^k = [\kappa_G(\mathbf{d}_{AA}^k); \kappa_G(\mathbf{d}_{AB}^k)]^\top,$$

$k+ = 1$

end

$$\mathbf{W}_F = \min(\widehat{w}_{N_{ij}}^k), \text{ with } i = 1, \dots, c; j = 1, \dots, n_s.$$

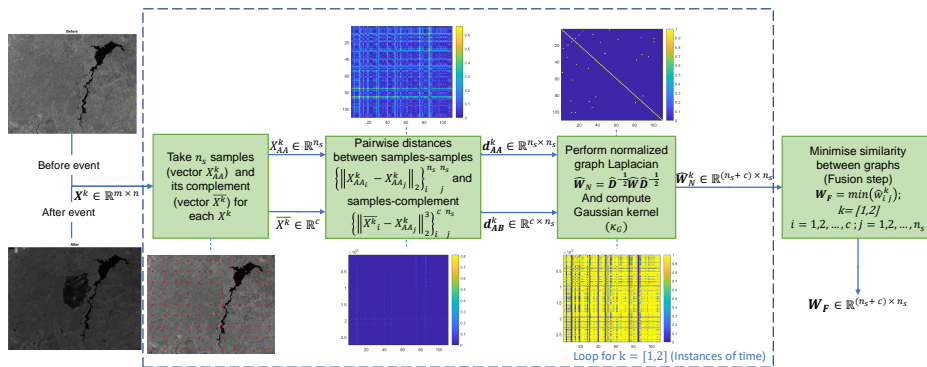


Fig. 1. Graph-based fusion. Where, k is the time of the event 1 (pre) and 2 (post), X^k is an image that represents a event, X_{AA}^k represents the samples from X^k , \bar{X}^k is the complement, \mathbf{d}_{AA}^k is the pairwise distance between the samples in X_{AA}^k , \mathbf{d}_{AB}^k is the pairwise distance between X_{AA}^k and \bar{X}^k , $\widehat{\mathbf{D}} = \text{Diag}(d_1, d_2, \dots, d_{n_s})$ with $d_i = \sum_j \widehat{w}_{ij}^k$ is the approximated degree matrix, and $\widehat{\mathbf{W}}_N^k$ is the normalized laplacian calculated by using the Nyström approximation.

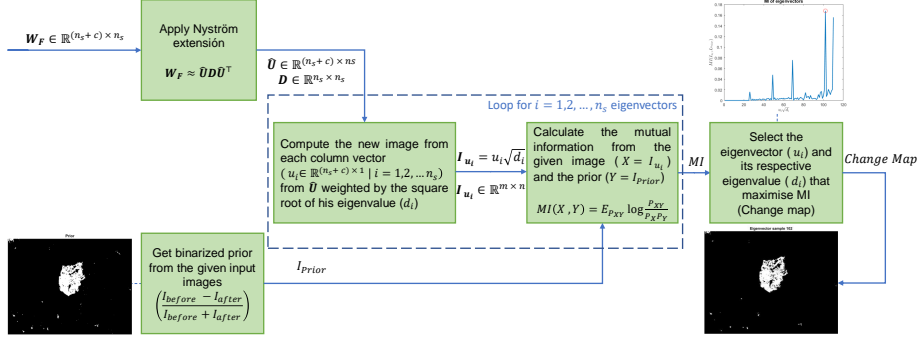


Fig. 2. Change detection. Where, \widehat{W}_F is the fused graph, \widehat{U} is the approximate eigenvectors and D is the eigenvalues.

preserve most of the information):

$$W_F = \min(\widehat{w}_{N_{ij}}^k), \text{ with } k = [1, 2],$$

where $w_{i,j}$ represents the weight of the node for each instance of time ($i = 1, 2, \dots, c; j = 1, 2, \dots, n_s$). In this sense, the learning of this approach is data driven (uses a few n_s samples to learn) and it will be restarted from scratch for each set of data.

3. APPLICATION OF GBF-CD FOR CHANGE DETECTION

3.1. Change detection scheme based on multi-temporal graph

To obtain the change map from the multi-temporal graph (section 2), we apply the scheme detailed in Figure 2. Here, the purpose is to attain the best match that reflects the change produced by any source. To do this, we use the eigenvectors from the GBF-CD as descriptors of the change. Nevertheless, the number of eigenvectors is equal to the samples (n_s) taken from the instances of time. Hence, we estimate the mutual information to identify the relevant eigenvector that captures the global change. The output in Figure 2 is a vector that contains the mutual information between the prior knowledge (difference image) and the change map generated by the eigenvectors of the GBF-CD. Finally the change map detected is the image-image (I_{u_i}) that maximizes the mutual information.

4. EXPERIMENTAL RESULTS AND DISCUSSION

4.1. Databases

Due to space limitations, we tested our approach on two datasets.: **Dataset A**: NIR band images (Figure 3 (a-b)) were acquired by the Thematic Mapper (TM) MS sensor of the Landsat-5 satellite. The scene represents an area including Lake Mulargia (Sardinia Island, Italy). The images consist of 573×479 pixels. The dates of acquisition were September 1995 (before the event) and July 1996 (after the event).

Dataset B: RED band images (Figure 3 (c-d)) were acquired by the Operational Land Image MS sensor of the Landsat-8 satellite. The area includes Lake Omodeo and a portion of Tirso River (Sardinia Island, Italy). The images consist of 965×742 pixels. The dates of acquisition were July 25, 2013 (before the event) and August 10, 2013 (after the event).

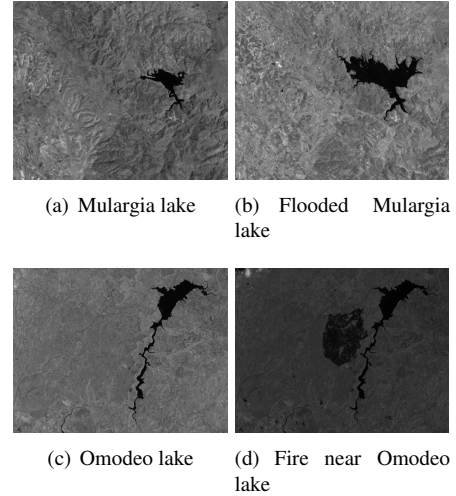


Fig. 3. Satellite images from the NIR band for the flood event (Dataset A) and from the red band for fire event (Dataset B).

4.2. Experimental set-up

We compare the proposed GBF-CD with state of the art methods: Rayleigh-Rice (rR) [6], Rayleigh-Rayleigh-Rice (rrR) [7], and the classical KittlerIllingsworth (KI) [5]. We evaluate relevant metrics in change detection such as: missed alarms (MA), false alarms (FA), precision (P), recall (R), Cohen's kappa (K) and overall error (OE).

The number of samples (n_s) was fixed at 92 and the standard deviations (σ) for the kernels were $\sigma_{lake}^1 = 2.5299 \times 10^{-10}$, $\sigma_{lake}^2 = 1.5561 \times 10^{-10}$, $\sigma_{fire}^1 = 2.793 \times 10^{-11}$ and $\sigma_{fire}^2 = 1.6533 \times 10^{-10}$, where the superscripts 1, 2 stands for pre and post event respectively. We set these values through

exhaustive grid-search using *MatLab*[®]2017a.

Table 1. Model Performance for dataset A.

Method	MA (%)	FA (%)	P	R	K	OE (%)
KI [5]	10.2425	1.0490	0.7229	0.8975	0.7941	1.3211
rR-EM [6]	5.7245	4.0147	0.4173	0.9427	0.5605	4.0653
rrR-EM [7]	10.1440	1.0637	0.7203	0.8985	0.7928	1.3324
GBF-CD	4.8504	0.3120	0.9029	0.9515	0.9242	0.4463

Table 2. Model Performance of dataset B.

Method	MA (%)	FA (%)	P	R	K	OE (%)
KI [5]	0	3.4291	0.5903	1	0.7262	3.2676
rR-EM [6]	0.0029	3.7382	0.5693	0.9999	0.7080	3.5623
rrR-EM [7]	0.0029	2.1449	0.6973	0.9999	0.8112	2.0440
GBF-CD	14.4217	0.1226	0.9718	0.8557	0.9059	0.7960

Table 1 shows the results for dataset A. We observe our approach outperforms the comparison methods for all metrics. Similarly, Table 2 tabulates the outcomes for dataset B. Although, the **KI** method achieves a perfect score for MA and recall (R), the **GBF-CD** outperforms the state-of-the-art methods in FA, P, K and OE.

Also, Figure 4 shows the behavior of each method in terms of MA (blue points), FA (red points) and correct changed pixels (green points). These results are remarkable, because we can see that probabilistic methods have a considerable number of FA in both datasets. Conversely, the **GBF-CD** deals well with this issue. FA is mostly generated by the nearly similar intensity of pixels between real changes regions and effects produced by the reflectance (i.e. weather variations, cloud density, daylight differences when the image was captured). The **GBF-CD** has some limitations. Firstly, for dataset A (see subfigure 4 (d)), we can observe that border of the change map is mainly composed by red points (FA). This is due to the neighboring pixels of the border have a similar intensity. Also, for dataset B (see figure 4 (h)), the **GBF-CD** is unable to detect minor changes in the edge of lake Omodeo and the artifact located in the upper-left corner. For this reason, there are some missed alarms (MA) represented by the blue points.

Further work includes: (i) to decrease the dependence of the results with respect to the number of selected samples for the Nyström extension, (ii) to select an alternative metric instead of Euclidean distance (ED) to increase the difference between intensities in MS images and avoid raising the ED to the power of three, (iii) to explore other kernel types.

5. CONCLUSIONS

In this paper, we introduced a change detection methodology (**GBF-CD**) based on graphs data fusion. Our main contribution is a “data-driven” framework. Our method models the dataset by finding eigenvectors of the normalized graph Laplacian and applying a mutual information based criteria to

obtain the relevant eigenvector that captures the change map. Experimental results showed that **GBF-CD** outperformed probabilistic threshold methods when we evaluated several metrics (MA, FA, R, P, K, OE) in two real cases of change detection in remote sensing images.

According to the previous results and analysis, we conclude that the **GBF-CD** is a promising and robust approach for detecting changes in remote sensing images.

Acknowledgments This work was funded by the OMICAS program: “Optimización Multiescala In-silico de Cultivos Agrícolas Sostenibles (Infraestructura y validación en Arroz y Caña de Azúcar)”, sponsored within the Colombian Scientific Ecosystem by The WORLD BANK, COLCIENCIAS, ICE-TEX, the Colombian Ministry of Education and the Colombian Ministry of Industry and Tourism under GRANT ID: FP44842-217-2018.

6. REFERENCES

- [1] Mauro Dalla Mura, Saurabh Prasad, Fabio Pacifici, Paulo Gamba, Jocelyn Chanussot, and Jón Atli Benediktsson, “Challenges and opportunities of multimodality and data fusion in remote sensing,” *Proceedings of the IEEE*, vol. 103, no. 9, pp. 1585–1601, 2015.
- [2] Dana Lahat, Tülay Adalı, and Christian Jutten, “Multimodal data fusion: an overview of methods, challenges, and prospects,” *Proceedings of the IEEE*, vol. 103, no. 9, pp. 1449–1477, 2015.
- [3] Amir Yavariabdi and Huseyin Kusetogullari, “Change detection in multispectral landsat images using multiobjective evolutionary algorithm,” *IEEE Geoscience and Remote Sensing Letters*, vol. 14, no. 3, pp. 414–418, 2017.
- [4] Mi Song, Yanfei Zhong, and Ailong Ma, “Change detection based on multi-feature clustering using differential evolution for landsat imagery,” *Remote Sensing*, vol. 10, no. 10, pp. 1664, 2018.
- [5] Josef Kittler and John Illingworth, “Minimum error thresholding,” *Pattern recognition*, vol. 19, no. 1, pp. 41–47, 1986.
- [6] Massimo Zanetti, Francesca Bovolo, and Lorenzo Bruzzone, “Rayleigh-rice mixture parameter estimation via em algorithm for change detection in multispectral images,” *IEEE Transactions on Image Processing*, vol. 24, no. 12, pp. 5004–5016, 2015.
- [7] Massimo Zanetti and Lorenzo Bruzzone, “A theoretical framework for change detection based on a compound multiclass statistical model of the difference image,” *IEEE Transactions on Geoscience and Remote Sensing*, vol. 56, no. 2, pp. 1129–1143, 2017.

To ensure the reproducibility of the proposed method, the code is publicly available at: <https://github.com/DavidJimenezS>

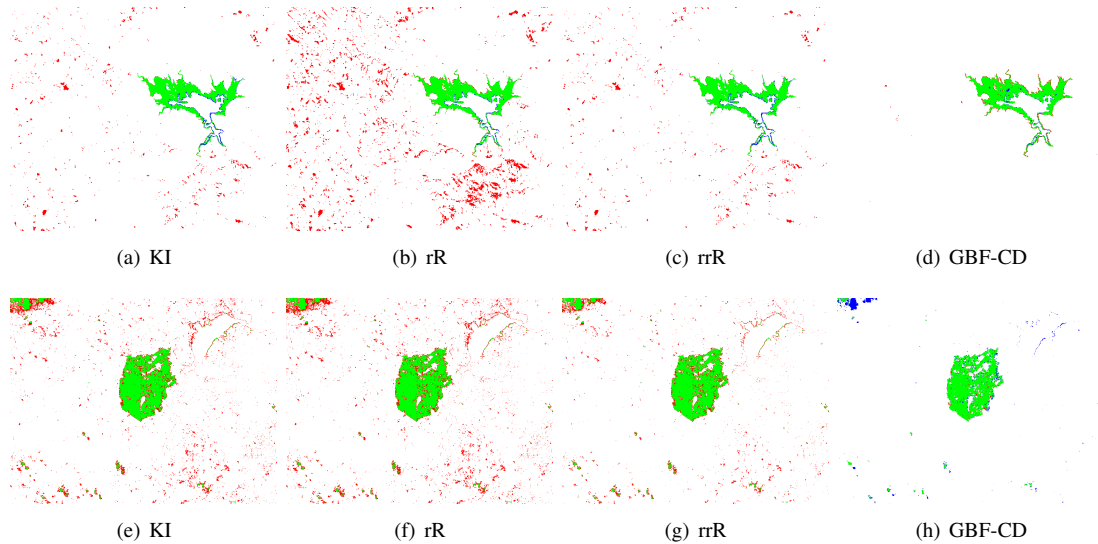


Fig. 4. Change map detected with respect to missed alarms (MA), false alarms (FA) and correct changed pixels (C).

- [8] Ammar Mian, Guillaume Ginolhac, Jean-Philippe Ovarlez, and Abdourrahmane Mahamane Atto, “New robust statistics for change detection in time series of multivariate sar images,” *IEEE Transactions on Signal Processing*, vol. 67, no. 2, pp. 520–534, 2018.
- [9] Redha Touati, Max Mignotte, and Mohamed Dahmane, “Multimodal change detection in remote sensing images using an unsupervised pixel pairwise based markov random field model,” *IEEE Transactions on Image Processing*, 2019.
- [10] Begüm Demir, Francesca Bovolo, and Lorenzo Bruzzone, “Classification of time series of multispectral images with limited training data,” *IEEE Transactions on Image Processing*, vol. 22, no. 8, pp. 3219–3233, 2013.
- [11] Ashish Ghosh, Niladri Shekhar Mishra, and Susmita Ghosh, “Fuzzy clustering algorithms for unsupervised change detection in remote sensing images,” *Information Sciences*, vol. 181, no. 4, pp. 699–715, 2011.
- [12] Turgay Celik, “Change detection in satellite images using a genetic algorithm approach,” *IEEE Geoscience and Remote Sensing Letters*, vol. 7, no. 2, pp. 386–390, 2010.
- [13] Maoguo Gong, Zhiqiang Zhou, and Jingjing Ma, “Change detection in synthetic aperture radar images based on image fusion and fuzzy clustering,” *IEEE Transactions on Image Processing*, vol. 21, no. 4, pp. 2141–2151, 2011.
- [14] Vladimir A Krylov, Gabriele Moser, Sebastiano B Serpico, and Josiane Zerubia, “False discovery rate approach to unsupervised image change detection,” *IEEE Transactions on Image Processing*, vol. 25, no. 10, pp. 4704–4718, 2016.
- [15] Zhunga Liu, Gang Li, Gregoire Mercier, You He, and Quan Pan, “Change detection in heterogenous remote sensing images via homogeneous pixel transformation,” *IEEE Transactions on Image Processing*, vol. 27, no. 4, pp. 1822–1834, 2017.
- [16] Rosa Mara Mnedez Parra Alfredo Caicedo Barrero, Graciela Wagner de Garca, “Introducción a la teoría de grafos,” vol. 1, pp. 1–12. Elizcom s.a.s, 2010.
- [17] Charless Fowlkes, Serge Belongie, Fan Chung, and Jitendra Malik, “Spectral grouping using the nystrom method,” *IEEE Transactions on Pattern Analysis and Machine Intelligence*, vol. 26, no. 2, pp. 214–225, 2004.
- [18] Geoffrey Iyer, Jocelyn Chanussot, and Andrea L Bertozzi, “A graph-based approach for feature extraction and segmentation of multimodal images,” in *2017 IEEE International Conference on Image Processing (ICIP)*. IEEE, 2017, pp. 3320–3324.